

# Deconfinement and Hadron Properties at Extremes of Temperature and Density\*

David Blaschke<sup>a</sup> and Craig D. Roberts<sup>b</sup>

<sup>a</sup>Fachbereich Physik, Universität Rostock, D-18051 Rostock, Germany

<sup>b</sup>Physics Division, Argonne National Laboratory, Argonne IL 60439-4843, USA

After introducing essential, qualitative concepts and results, we discuss the application of Dyson-Schwinger equations to QCD at finite  $T$  and  $\mu$ . We summarise the calculation of the critical exponents of two-light-flavour QCD using the chiral and thermal susceptibilities; and an algebraic model that elucidates the origin of an anticorrelation between the  $\mu$ - and  $T$ -dependence of a range of meson properties. That model also provides an algebraic understanding of why the finite- $T$  behaviour of bulk thermodynamic properties is mirrored in their  $\mu$ -dependence, and why meson masses decrease with  $\mu$  even though  $f_\pi$  and  $-\langle\bar{q}q\rangle$  increase. The possibility of diquark condensation is canvassed. Its realisation is uncertain because it is contingent upon an assumption about the quark-quark scattering kernel that is demonstrably false in some applications; e.g., it predicts the existence of coloured diquarks in the strong interaction spectrum, which are not observed.

## 1. DYSON-SCHWINGER EQUATIONS

The Dyson-Schwinger equations (DSEs) provide a Poincaré invariant, continuum approach to solving quantum field theories. There are many familiar examples, among them: the gap equation in superconductivity; and the Bethe-Salpeter equation (BSE) and covariant Fadde'ev equation, which describe relativistic 2- and 3-body bound states. The DSEs are a system of coupled integral equations and a truncation is necessary to obtain a tractable problem. The simplest truncation scheme is a weak-coupling expansion, which generates every diagram in perturbation theory. Hence, in the intelligent application of DSEs to QCD, there is always a tight constraint on the ultraviolet behaviour. That is crucial in extrapolating into the infrared, and in developing uniformly valid, efficacious, symmetry-preserving truncations.

The task of development is not a purely numerical one, and neither is it always obviously systematic. For some, this last point diminishes the appeal of the approach. However, with growing community involvement and interest, the qualitatively robust results and intuitive understanding that the DSEs can provide is becoming clear. Indeed, those

---

\*A combined summary of two presentations, one by each author. This work was supported by the US Department of Energy, Nuclear Physics Division, under contract number W-31-109-ENG-38; the National Science Foundation under grant no. INT-9603385; Deutscher Akademischer Austauschdienst; and benefited from the resources of the National Energy Research Scientific Computing Center.

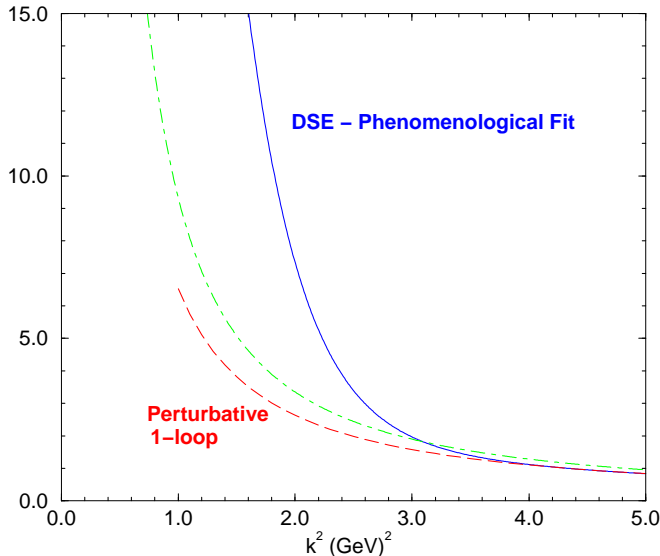


Figure 1.  $\mathcal{G}(k^2)/k^2$  from a solution [ 3] of the gluon DSE (dash-dot line) compared with the one-loop perturbative result (dashed line) and a fit (solid line) obtained following the method of Ref. [ 4]; i.e., requiring that the gluon propagator lead, via the quark DSE, to a good description of a range of hadron observables.

familiar with the application of DSEs in the late-70s and early-80s might be surprised with the progress that has been made.

The DSEs have been used extensively [ 1] in developing an understanding of confinement and dynamical chiral symmetry breaking (DCSB), and their wide application [ 2] to the description of hadron properties in terms of their quark and gluon constituents is built upon that success. In understanding and unifying these phenomena, the DSEs point to the key role played by the necessary, momentum-dependent dressing of the elementary propagators and vertices in QCD.

### 1.1. Gluon propagator

Important in the application of DSEs is the gluon propagator, which at  $T = 0$  has the form:

$$g^2 D_{\mu\nu}(k) = \left( \delta_{\mu\nu} - \frac{k_\mu k_\nu}{k^2} \right) \frac{\mathcal{G}(k^2)}{k^2}, \quad \mathcal{G}(k^2) := \frac{g^2}{[1 + \Pi(k^2)]}, \quad (1)$$

where  $\Pi(k^2)$  is the vacuum polarisation that contains all the dynamical information about gluon propagation. Studies of the gluon DSE have been reported by many authors [ 1] with the conclusion that, if the ghost-loop is not significant, then the charge-antiscreening 3-gluon vertex dominates and, relative to the free gauge boson propagator, the dressed gluon propagator is significantly enhanced in the vicinity of  $k^2 = 0$ . The enhancement persists to  $k^2 \sim 1\text{-}2 \text{ GeV}^2$ , where a perturbative analysis becomes quantitatively reliable. In the neighbourhood of  $k^2 = 0$  the enhancement can be represented [ 3] as a regularisation of  $1/k^4$  as a distribution, and this behaviour is illustrated in Fig.1. A dressed-gluon propagator of this type generates DCSB and confinement *without* fine-tuning. (We identify confinement as the absence of a Lehmann representation for coloured propagators, with

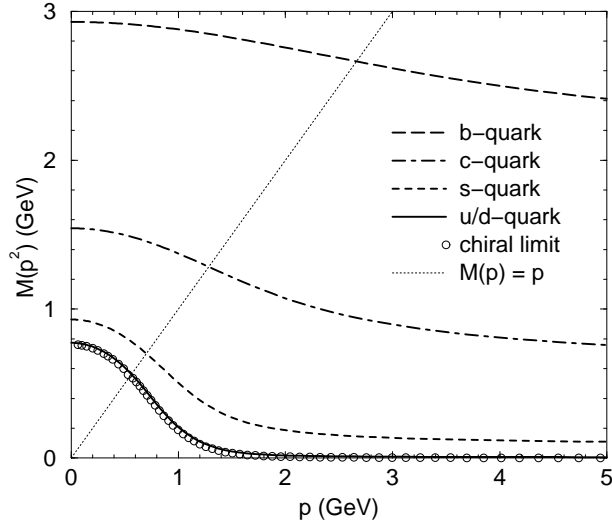


Figure 2.  $M(p^2) := B(p^2)/A(p^2)$  obtained in solving the quark DSE. The solution of  $M^2(p^2) = p^2$  defines  $M^E$ , the Euclidean constituent-quark mass.

the obvious analogue for other coloured n-point functions.)

## 1.2. Quark propagator

At  $T = 0 = \mu$  in a covariant gauge the dressed-quark propagator has the form

$$S(p) := \frac{1}{i\gamma \cdot p + \Sigma(p)} := \frac{1}{i\gamma \cdot p A(p^2) + B(p^2)}. \quad (2)$$

$\Sigma(p)$  is the renormalised dressed-quark self energy, which satisfies

$$\Sigma(p) = (Z_2 - 1) i\gamma \cdot p + Z_4 m^\zeta + Z_1 \int_q^\Lambda g^2 D_{\mu\nu}(p - q) \frac{\lambda^a}{2} \gamma_\mu S(q) \Gamma_\nu^a(q, p), \quad (3)$$

where  $\Gamma_\nu^a(q; p)$  is the dressed-quark-gluon vertex,  $m^\zeta$  is the current-quark mass,  $\zeta$  is the renormalisation point, and  $\int_q^\Lambda := \int^\Lambda d^4q / (2\pi)^4$  represents mnemonically a *translationally-invariant* regularisation of the integral, with  $\Lambda$  the regularisation mass-scale. Using  $\mathcal{G}(k^2)$  similar to that depicted in Fig. 1 and current-quark masses corresponding to

$$\begin{array}{cccc} m_{u/d}^{1\text{ GeV}} & m_s^{1\text{ GeV}} & m_c^{1\text{ GeV}} & m_b^{1\text{ GeV}} \\ 6.6\text{ MeV} & 140\text{ MeV} & 1.0\text{ GeV} & 3.4\text{ GeV} \end{array} \quad (4)$$

one obtains [ 5] the dressed-quark mass function depicted in Fig. 2.

For light quarks ( $u$ ,  $d$  and  $s$ ) there are two distinct domains: perturbative and non-perturbative. In the perturbative domain the magnitude of  $M(p^2)$  is governed by the the current-quark mass. For  $p^2 < 1\text{ GeV}^2$  the mass-function rises sharply. This is the nonperturbative domain where the magnitude of  $M(p^2)$  is determined by the DCSB mechanism; i.e., the enhancement in the dressed-gluon propagator. This emphasises that DCSB is more than just a nonzero value of the quark condensate in the chiral limit!

For a given flavour, the ratio  $\mathcal{L}_f := M_f^E/m_f^\zeta$  is a single, quantitative measure of the importance of the DCSB mechanism in modifying that quark's propagation characteristics. As illustrated in Eq. (5),

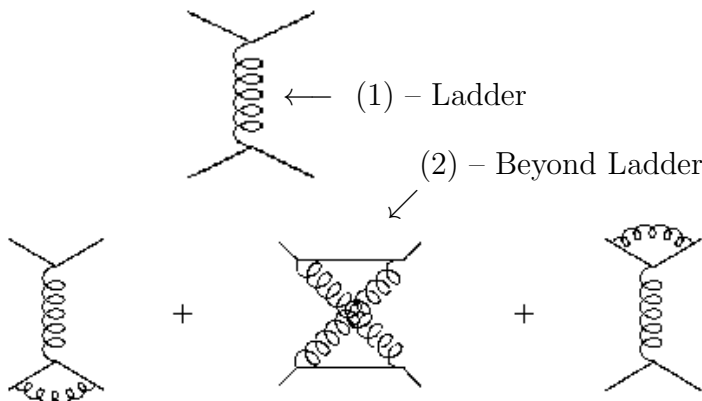


Figure 3. First two orders in a systematic expansion [ 7] of the quark-antiquark scattering kernel. In this expansion, the propagators are dressed but the vertices are bare.

flavour	$u/d$	$s$	$c$	$b$	$t$
$\frac{M^E}{m_{\zeta \sim 20 \text{ GeV}}}$	150	10	2.3	1.4	$\rightarrow 1$

(5)

this ratio provides for a natural classification of quarks as either light or heavy. For light-quarks  $\mathcal{L}_f$  is characteristically 10-100 while for heavy-quarks it is only 1-2. The values of  $\mathcal{L}_f$  signal the existence of a characteristic DCSB mass-scale:  $M_\chi$ . At  $p^2 > 0$  the propagation characteristics of a flavour with  $m_f^\zeta < M_\chi$  are altered significantly by the DCSB mechanism, while for flavours with  $m_f^\zeta \gg M_\chi$  it is irrelevant, and explicit chiral symmetry breaking dominates. It is apparent from Eq. (5) that  $M_\chi \sim 0.2 \text{ GeV} \sim \Lambda_{\text{QCD}}$ . This forms a basis for many simplifications in the study of heavy-meson observables.[ 6]

### 1.3. Hadrons are bound states

The properties of hadrons can be understood by studying covariant bound state equations: the Bethe-Salpeter equation (BSE) for mesons and the covariant Fadde'ev equation for baryons. The mesons have been studied most extensively and their internal structure is described by a Bethe-Salpeter amplitude obtained as a solution of

$$[\Gamma_H(k; P)]_{tu} = \int_q^\Lambda [\chi_H(q; P)]_{sr} K_{tu}^{rs}(q, k; P), \quad (6)$$

where  $\chi_H(q; P) := \mathcal{S}(q_+) \Gamma_H(q; P) \mathcal{S}(q_-)$ ;  $\mathcal{S}(q) := \text{diag}(S_u(q), S_d(q), S_s(q), \dots)$ ;  $q_+ = q + \eta_P P$ ,  $q_- = q - (1 - \eta_P) P$ , with  $P$  the total momentum of the bound state and observables independent of  $\eta_P$ ; and  $r, \dots, u$  represent colour-, Dirac- and flavour-matrix indices.

In Eq.(6),  $K$  is the renormalised, fully-amputated, quark-antiquark scattering kernel and important in the successful application of DSEs is that it has a systematic skeleton expansion in terms of the elementary, dressed-particle Schwinger functions; e.g., the dressed-quark and -gluon propagators. The particular expansion depicted in Fig. 3, with its analogue for the kernel in the quark DSE, provides a means of constructing a kernel that, order-by-order in the number of vertices, ensures the preservation of vector and axial-vector Ward-Takahashi identities and hence Goldstone's theorem.

### 1.4. Phenomenological applications

Some of the many applications of DSEs to the calculation of hadron observables at  $T = 0 = \mu$  are summarised in Refs. [ 2] so here we make only two brief observations. Using

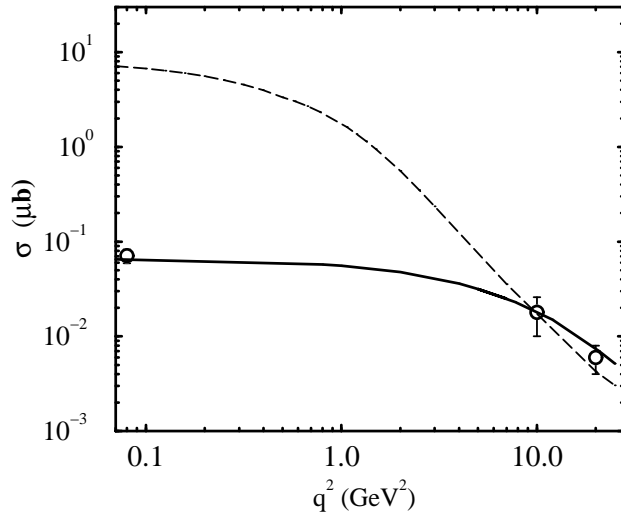


Figure 4.  $\psi$ -meson electroproduction cross section: solid line; the dashed line is the  $\rho$ -meson cross section for comparison. The data are from Refs. [ 10].

the DSEs one obtains a mass formula for pseudoscalar mesons that unifies the small and large current-quark mass regimes. For mesons composed of quarks with small current-quark masses the formula yields [ 4] the Gell-Mann–Oakes–Renner relation. However, when the current-quark mass of one or both of the constituents is large, the formula predicts [ 8] that the meson mass increases linearly with the current-quark mass. In model studies [ 5] the linear increase is dominant for masses as low as that of the  $s$ -quark. The approach has also been extensively employed in the study of scattering processes, and one example is the calculation [ 9] of the cross section for the diffractive electroproduction of vector mesons. This application makes the striking prediction, confirmed by recent data, that although two-orders of magnitude smaller than the  $\rho$ -meson cross section at the photoproduction point, the  $\psi$ -meson cross section is equal to that of the  $\rho$ -meson at  $Q^2 = 15 \text{ GeV}^2$ , Fig. 4.

## 2. FINITE TEMPERATURE AND CHEMICAL POTENTIAL

The contemporary application of DSEs at finite temperature and chemical potential is a straightforward extension of the  $T = 0 = \mu$  studies. The direct approach is to develop a finite- $T$  extension of *Ansätze* for the dressed-gluon propagator and then solve the quark DSE. Having the dressed-quark and -gluon propagators, the response of bound states to increases in  $T$  and  $\mu$  can be calculated. As a nonperturbative approach that allows the simultaneous study of confinement and DCSB, the DSEs have a significant overlap with lattice simulations: each quantity that can be estimated using lattice simulations can also be calculated using DSEs. That means they can be used to check the lattice simulations, and importantly, that lattice simulations can be used to constrain their model-dependent aspects. Once agreement is obtained on the common domain, the DSEs can be used to explore phenomena presently inaccessible to lattice simulations.

The renormalised dressed-quark propagator at finite- $(T, \mu)$  has the form

$$S^{-1}(\vec{p}, \tilde{\omega}_k) = i\vec{\gamma} \cdot \vec{p} A(\vec{p}, \tilde{\omega}_k) + i\gamma_4 \tilde{\omega}_k C(\vec{p}, \tilde{\omega}_k) + B(\vec{p}, \tilde{\omega}_k) \quad (7)$$

where  $\tilde{\omega}_k := \omega_k + i\mu$  with  $\omega_k = (2k + 1)\pi T$ ,  $k \in \mathbf{Z}$ , and satisfies the DSE

$$S^{-1}(\vec{p}, \tilde{\omega}_k) = Z_2^A i\vec{\gamma} \cdot \vec{p} + Z_2 (i\gamma_4 \tilde{\omega}_k + m_{\text{bm}}) + \Sigma'(\vec{p}, \tilde{\omega}_k); \quad (8)$$

where the regularised self energy is

$$\Sigma'(\vec{p}, \tilde{\omega}_k) = i\vec{\gamma} \cdot \vec{p} \Sigma'_A(\vec{p}, \tilde{\omega}_k) + i\gamma_4 \tilde{\omega}_k \Sigma'_C(\vec{p}, \tilde{\omega}_k) + \Sigma'_B(\vec{p}, \tilde{\omega}_k), \quad (9)$$

$$\Sigma'_F(\vec{p}, \tilde{\omega}_k) = \int_{l,q}^{\bar{\Lambda}} \frac{4}{3} g^2 D_{\mu\nu}(\vec{p} - \vec{q}, \tilde{\omega}_k - \tilde{\omega}_l) \frac{1}{4} \text{tr} [\mathcal{P}_F \gamma_\mu S(\vec{q}, \tilde{\omega}_l) \Gamma_\nu(\vec{q}, \tilde{\omega}_l; \vec{p}, \tilde{\omega}_k)], \quad (10)$$

$\int_{l,q}^{\bar{\Lambda}} := T \sum_{l=-\infty}^{\infty} \int \frac{d^3 q}{(2\pi)^3}$  and  $\mathcal{P}_A := -(Z_1^A/p^2)i\gamma \cdot p$ ,  $\mathcal{P}_B := Z_1$ ,  $\mathcal{P}_C := -(Z_1/\tilde{\omega}_k)i\gamma_4$ . The complex scalar functions:  $A(\vec{p}, \tilde{\omega}_k)$ ,  $B(\vec{p}, \tilde{\omega}_k)$  and  $C(\vec{p}, \tilde{\omega}_k)$  satisfy:  $\mathcal{F}(\vec{p}, \tilde{\omega}_k)^* = \mathcal{F}(\vec{p}, \tilde{\omega}_{-k-1})$ ,  $\mathcal{F} = A, B, C$ , and although not explicitly indicated they are functions only of  $|\vec{p}|^2$  and  $\tilde{\omega}_k^2$ . The dependence of these functions on their arguments has important consequences in QCD. It can provide a mechanism for quark confinement and is the reason why bulk thermodynamic quantities, such as the pressure and entropy, approach their ultrarelativistic limits slowly.

### 2.1. Chiral phase transition at $\mu = 0$

One order parameter for the chiral symmetry restoration transition is the quark condensate, defined via the renormalised dressed-quark propagator:

$$-\langle \bar{q}q \rangle_\zeta^0 = \lim_{\bar{\Lambda} \rightarrow \infty} Z_4(\zeta^2, \bar{\Lambda}^2) N_c \int_{l,q}^{\bar{\Lambda}} \text{tr}_{\text{Dirac}} [S_{\hat{m}=0}(q)]. \quad (11)$$

Since  $\text{tr}_{\text{Dirac}} [S_{\hat{m}=0}(q)] \propto B(\vec{p}, \tilde{\omega}_k)$ , a simpler and equivalent order parameter is

$$\mathcal{X}(t, h) := \text{Re } B_0(\vec{p} = 0, \tilde{\omega}_0); \quad t := \frac{T}{T_c} - 1, \quad h := \frac{m^\zeta}{T}, \quad (12)$$

which makes it clear that the zeroth Matsubara mode determines the character of the chiral phase transition. (An order parameter for confinement, valid for both light- and heavy-quarks, was introduced in Ref. [11]. It is a single, quantitative measure of whether or not a Schwinger function has a Lehmann representation, and has been used [12] to striking effect in QED<sub>3</sub>.)

The chiral transition is completely characterised by two critical exponents:  $\beta$ ,  $\delta$ , which can be extracted from the behaviour of the chiral and thermal susceptibilities: [13]

$$\chi_h(t, h) := \left. \frac{\partial \mathcal{X}(t, h)}{\partial h} \right|_t, \quad \chi_t(t, h) := \left. \frac{\partial \mathcal{X}(t, h)}{\partial t} \right|_h. \quad (13)$$

As a function of  $T$  the susceptibilities have a peak, which defines the pseudocritical points:  $t_{\text{pc}}^h$ ,  $t_{\text{pc}}^t$ , and because the correlation length is infinite at a second order transition it follows that

$$\chi_h^{\text{pc}} := \chi_h(t_{\text{pc}}^h, h) \propto h^{-z_h}, \quad z_h := 1 - \frac{1}{\delta}, \quad \chi_t^{\text{pc}} := \chi_t(t_{\text{pc}}^t, h) \propto h^{-z_t}, \quad z_t := \frac{1}{\beta\delta} (1 - \beta). \quad (14)$$

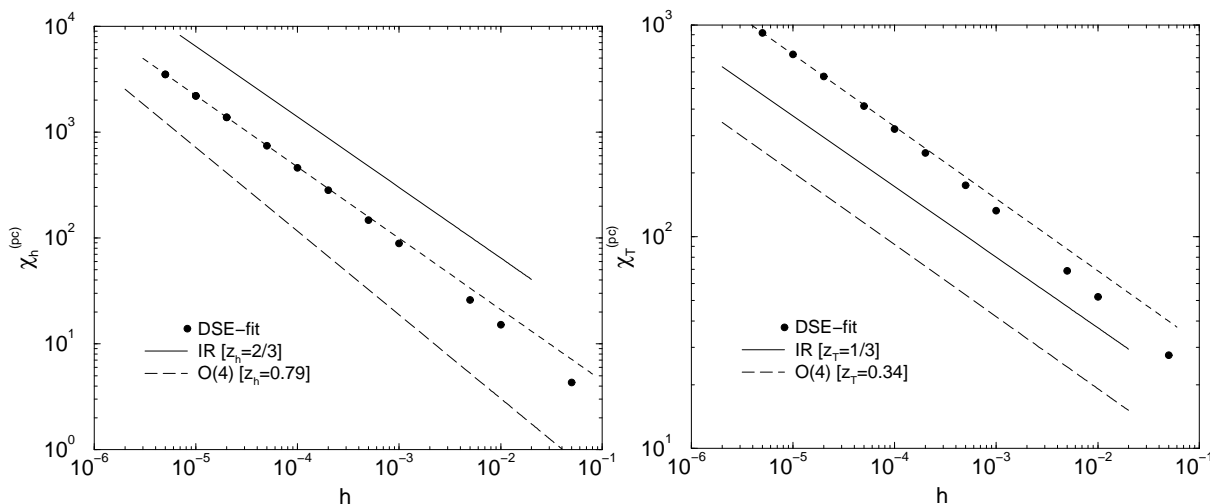


Figure 5. Behaviour of the susceptibilities in the DSE model of two-light-flavour QCD illustrated in Fig. 1,[ 14] which is a minor modification of that in Ref. [ 4]:  $\omega \rightarrow 0.6$  GeV, that provides a slightly better description of  $\pi$  and  $K$  properties. The critical temperature is  $T_c^{\mathcal{X}} = 152$  MeV and the critical exponents take mean-field values:  $z_h = 0.67$ ,  $z_t = 0.33$ ; i.e.,  $\beta = 0.5$ ,  $\delta = 3.0$ , as might be anticipated because at long-range the interaction  $\sim \text{const.}$  in configuration space. The other curves illustrate the slopes characterising mean-field (labelled IR) and  $O(4)$  critical exponents.

Hence the critical exponents can be obtained by plotting  $\log_{10} \chi^{\text{pc}}$  vs.  $\log_{10} h$ , as depicted in Fig. 5. This figure makes one thing abundantly clear: very small values of the current-quark mass must be used to obtain accurate values of the critical exponents. If one retains only those values  $5 \times 10^{-4} \lesssim h \lesssim 5 \times 10^{-2}$  then an apparently good linear fit yields:  $z_h = 0.78$ ,  $z_t = 0.40$ , or  $\beta = 0.36$ ,  $\delta = 4.5$ , which are quite close to the values of the  $O(4)$  model. The small values of the current-quark mass we require to accurately estimate the critical exponents are inaccessible in contemporary lattice simulations.

## 2.2. $T$ and $\mu$ nonzero

This is a difficult problem and the most complete study [ 15] to date employs a simple *Ansatz* for the dressed-gluon propagator that exhibits only the infrared enhancement suggested by Ref. [ 3]:

$$g^2 D_{\mu\nu}(\vec{p}, \Omega_k) = \left( \delta_{\mu\nu} - \frac{p_\mu p_\nu}{|\vec{p}|^2 + \Omega_k^2} \right) 2\pi^3 \frac{\eta^2}{T} \delta_{k0} \delta^3(\vec{p}), \quad (15)$$

with  $\Omega_k = 2k\pi T$  and  $\eta$  a mass-scale. It is an infrared-dominant model and does not represent well the behaviour of  $D_{\mu\nu}(\vec{p}, \Omega_k)$  away from  $|\vec{p}|^2 + \Omega_k^2 \approx 0$ . Consequently some model-dependent artefacts arise. However, there is significant merit in its simplicity and, since the artefacts are easily identified, the model remains useful as a means of elucidating many of the qualitative features of more sophisticated *Ansätze*.

Using Eq. (15) and the rainbow truncation [ $\Gamma_\mu \rightarrow \gamma_\mu$  in Eq. (10)], the quark DSE is [ 7]

$$S^{-1}(\vec{p}, \omega_k) = S_0^{-1}(\vec{p}, \tilde{\omega}_k) + \frac{1}{4} \eta^2 \gamma_\nu S(\vec{p}, \tilde{\omega}_k) \gamma_\nu, \quad (16)$$

and we see that the simplicity of the *Ansatz* allows the reduction of an integral equation to an algebraic equation. Its solution exhibits many of the qualitative features of more sophisticated models.

In the chiral limit Eq. (16) has two qualitatively distinct solutions. The Nambu-Goldstone solution, with

$$B(\tilde{p}_k) = \begin{cases} \sqrt{\eta^2 - 4\tilde{p}_k^2}, & \text{Re}(\tilde{p}_k^2) < \frac{\eta^2}{4}, \\ 0, & \text{otherwise} \end{cases}, \quad C(\tilde{p}_k) = \begin{cases} 2, & \text{Re}(\tilde{p}_k^2) < \frac{\eta^2}{4}, \\ \frac{1}{2} \left( 1 + \sqrt{1 + \frac{2\eta^2}{\tilde{p}_k^2}} \right), & \text{otherwise} \end{cases}, \quad (17)$$

where  $\tilde{p}_l := (\vec{p}, \tilde{\omega}_l)$ , describes a phase of the model in which: 1) chiral symmetry is dynamically broken, because one has a nonzero quark mass-function,  $B(\tilde{p}_k)$ , in the absence of a current-quark mass; and 2) the dressed-quarks are confined, because the propagator described by these functions does not have a Lehmann representation. The alternative Wigner solution, for which

$$\hat{B}(\tilde{p}_k) \equiv 0, \quad \hat{C}(\tilde{p}_k) = \frac{1}{2} \left( 1 + \sqrt{1 + \frac{2\eta^2}{\tilde{p}_k^2}} \right), \quad (18)$$

describes a phase of the model with neither DCSB nor confinement.

The relative stability of the different phases is measured by a  $(T, \mu)$ -dependent vacuum pressure difference:  $\mathcal{B}(T, \mu)$ .  $\mathcal{B}(T, \mu) = 0$  defines the phase boundary, and the deconfinement and chiral symmetry restoration transitions are coincident. For  $\mu = 0$  the transition is second order and the critical temperature is  $T_c^0 = 0.159 \eta$ , which using the value of  $\eta = 1.06 \text{ GeV}$  obtained by fitting the  $\pi$  and  $\rho$  masses corresponds to  $T_c^0 = 0.170 \text{ GeV}$ . This is only 12% larger than the value reported in Sec. 2.1, and the order of the transition is the same. For any  $\mu \neq 0$  the transition is first-order. For  $T = 0$  the critical chemical potential is  $\mu_c^0 = 0.3 \text{ GeV}$ , which is  $\approx 30\%$  smaller than the result in Ref. [16]. The discontinuity in the order parameter vanishes at  $\mu = 0$ .

The quark pressure is easily calculated and is depicted in Fig. 6. Confinement means that  $P_q \equiv 0$  in the confined domain. In the deconfined domain it approaches the ultrarelativistic, free particle limit,  $P_{\text{UR}}$ , at large values of  $T$  and  $\mu$  but the approach is slow. For example, at  $T \sim 2T_c^0$ , or  $\mu \sim 3\mu_c^0$ ,  $P_q$  is only  $0.5 P_{\text{UR}}$ . This feature results from the persistence of momentum dependent modifications of the quark propagator into the deconfined domain, as evident with  $C \neq 1$  in Eq. (18). The figure also highlights the ‘‘mirroring’’ of finite- $T$  behaviour in the  $\mu$ -dependence of the bulk thermodynamic quantities.

The vacuum quark condensate is given by the simple expression [17]

$$-\langle \bar{q}q \rangle = \eta^3 \frac{8N_c}{\pi^2} \bar{T} \sum_{l=0}^{l_{\text{max}}} \int_0^{\bar{\Lambda}_l} dy y^2 \text{Re} \left( \sqrt{\frac{1}{4} - y^2 + \bar{\mu}^2 - \bar{\omega}_l^2 - 2i\bar{\mu}\bar{\omega}_l} \right) : \quad (19)$$

$\bar{T} = T/\eta$ ,  $\bar{\mu} = \mu/\eta$ ;  $l_{\text{max}}$  is the largest value of  $l$  for which  $\bar{\omega}_{l_{\text{max}}}^2 \leq (1/4) + \bar{\mu}^2$  and this also specifies  $\omega_{l_{\text{max}}}$ ,  $\bar{\Lambda}^2 = \bar{\omega}_{l_{\text{max}}}^2 - \bar{\omega}_l^2$ ,  $\bar{p}_l = (\vec{y}, \bar{\omega}_l + i\bar{\mu})$ . At  $T = 0 = \mu$ ,  $(-\langle \bar{q}q \rangle) = \eta^3/(80\pi^2) = (0.11\eta)^3$ . Obvious from Eq. (19) is that  $(-\langle \bar{q}q \rangle)$  decreases continuously to zero with  $T$  but *increases* with  $\mu$ , up to a critical value of  $\mu_c(T)$  when it drops discontinuously to zero. This behaviour is driven by the combination  $\mu^2 - \omega_l^2$  and is exhibited by the calculated result depicted in Fig. 7. In the chiral limit one also has the simple expression

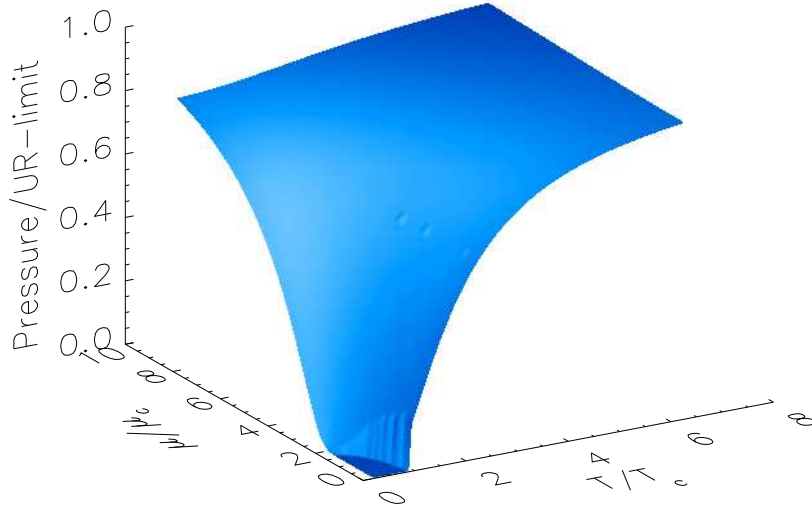


Figure 6. The quark pressure,  $P_q(\bar{T}, \bar{\mu})$ , normalised to the free, massless (or Ultra-Relativistic) result.

$$f_\pi^2 = \eta^2 \frac{16N_c}{\pi^2} \bar{T} \sum_{l=0}^{l_{\max}} \frac{\bar{\Lambda}_l^3}{3} \left( 1 + 4\bar{\mu}^2 - 4\bar{\omega}_l^2 - \frac{8}{5}\bar{\Lambda}_l^2 \right). \quad (20)$$

It too involves the combination  $\mu^2 - \omega_l^2$  and without calculation Eq. (20) indicates that  $f_\pi$  will *decrease* with  $T$  and *increase* with  $\mu$ , as exhibited by calculated result depicted in Fig. 7. These results confirm those obtained [ 11, 16] with more sophisticated *Ansätze*, and in doing so provide for their algebraic elucidation: the behaviour is a consequence of the necessary momentum dependence of the dressed-quark self energy.

The  $(T, \mu)$ -response of meson masses is determined by the ladder BSE

$$\Gamma_M(\tilde{p}_k; \check{P}_\ell) = -\frac{\eta^2}{4} \text{Re} \left\{ \gamma_\mu S(\tilde{p}_i + \frac{1}{2}\check{P}_\ell) \Gamma_M(\tilde{p}_i; \check{P}_\ell) S(\tilde{p}_i - \frac{1}{2}\check{P}_\ell) \gamma_\mu \right\}, \quad (21)$$

where  $\check{P}_\ell := (\vec{P}, \Omega_\ell)$ , with the bound state mass obtained by considering  $\check{P}_{\ell=0}$ . In this truncation the  $\omega$ - and  $\rho$ -mesons are degenerate. The calculated mass of the  $\pi$ - and  $\rho$ -mesons is depicted in Fig. 8. The behaviour is easily understood by again considering the chiral limit where the mass of the longitudinal component of the  $\rho$ -meson is

$$M_\rho^2 = \frac{1}{2}\eta^2 - 4(\mu^2 - \pi^2 T^2). \quad (22)$$

The characteristic combination  $\mu^2 - \pi^2 T^2$  appears again. It is responsible for the anti-correlation between the response of  $M_\rho$  to  $T$  and its response to  $\mu$ , and that  $M_\rho^2$  rises linearly with  $T^2$  for  $\mu = 0$ , just like a gauge-boson Debye mass. The mass of the transverse component of the vector meson is insensitive to  $T$  and  $\mu$ .

In a 2-flavour, free-quark gas at  $T = 0$  the baryon number density is  $\rho_B = 2\mu^3/(3\pi^2)$ , by which gauge nuclear matter density,  $\rho_0 = 0.16 \text{ fm}^{-3}$ , corresponds to  $\mu = \mu_0 := 260 \text{ MeV} = 0.245 \eta$ . At this chemical potential the algebraic model yields

$$M_\rho(\mu_0) \approx 0.75M_\rho(\mu = 0) \quad , \quad M_\phi(\mu_0) \approx 0.85M_\phi(\mu = 0), \quad (23)$$

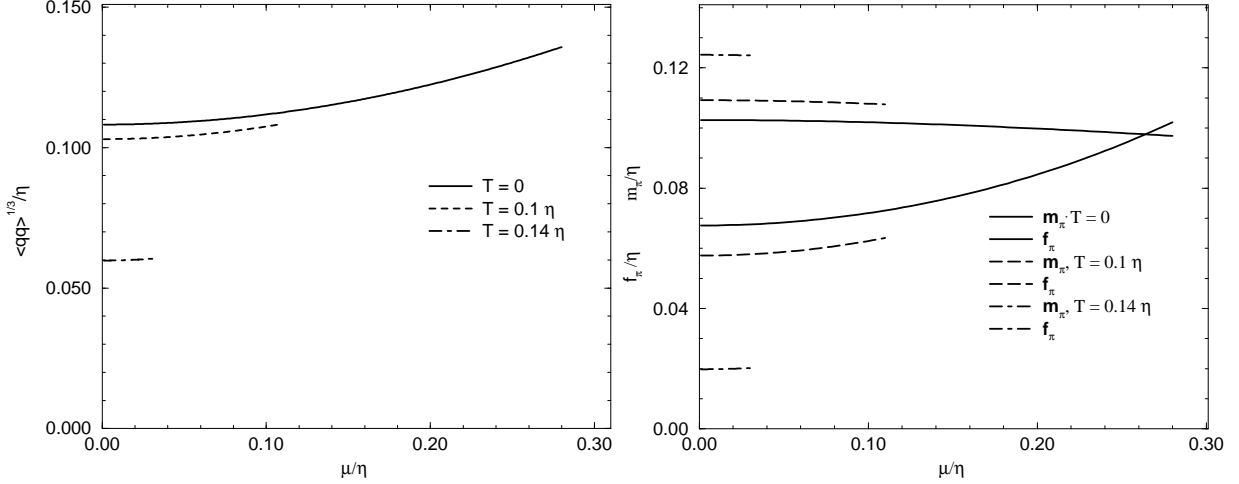


Figure 7.  $-\langle\bar{q}q\rangle$ ,  $f_\pi$  and  $m_\pi$  as a function of  $\mu$  for a range of values of  $T$ .  $m_\pi$  is only weakly sensitive to changes in  $\mu$  and  $T$  because of mutual cancellations between the effects of these intensive variables on  $-\langle\bar{q}q\rangle$  and  $f_\pi$ . That is a result of Goldstone's theorem; i.e., the preservation of the axial-vector Ward-Takahashi identity.

where  $M_\phi(\mu=0) = 1.02 \text{ GeV}$  for  $m_s = 180 \text{ MeV}$ . The study of Ref. [16] indicates that a more realistic representation of the ultraviolet behaviour of the dressed-gluon propagator expands the horizontal scale in Fig.8, with the critical chemical potential increased by 25%. This suggests that a better estimate is obtained by evaluating the mass at  $\mu'_0 = 0.20\eta$ , which yields

$$M_\rho(\mu'_0) \approx 0.85M_\rho(\mu=0) \quad , \quad M_\phi(\mu'_0) \approx 0.90M_\phi(\mu=0) ; \quad (24)$$

a small, quantitative modification. The difference between Eqs. (23) and (24) is a measure of the theoretical uncertainty in the estimates in each case. Pursuing this suggestion further,  $\mu_2 = \mu'_0 \sqrt[3]{2}$ , corresponds to  $2\rho_0$ , at which point  $M_\omega = M_\rho \approx 0.72 M_\rho(\mu=0)$  and  $M_\phi \approx 0.85 M_\phi(\mu=0)$ , while at the  $T=0$  critical chemical potential, which corresponds to approximately  $3\rho_0$  in Ref. [16],  $M_\omega = M_\rho \approx 0.65 M_\rho(\mu=0)$  and  $M_\phi \approx 0.80 M_\phi(\mu=0)$ . These are the maximum possible reductions in the meson masses.

This simple model preserves the momentum-dependence of gluon and quark dressing, which is an important qualitative feature of more sophisticated studies. Its simplicity means that many of the consequences of that dressing can be understood algebraically. For example, it elucidates the origin of an anticorrelation, found for a range of quantities, between their response to increasing  $T$  and that to increasing  $\mu$ . That makes clear why the transition to a QGP is second order with increasing  $T$  and first order with  $\mu$ . Further it provides an algebraic explanation of why the  $(T, \mu)$ -dependence of  $(-\langle\bar{q}q\rangle)$  and  $f_\pi$  must be *opposite* to that of  $M_\rho$ .

### 3. DIQUARKS

It is not implausible that diquark (quark-quark) correlations play an important role in the strong interaction. To see why, consider the class of models that can be characterised by an effective interaction of the form:

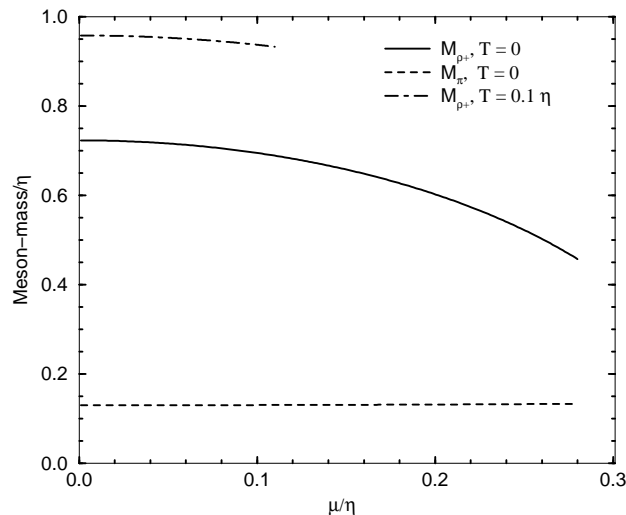


Figure 8.  $M_\rho = M_\omega$  and  $m_\pi$  as a function of  $\bar{\mu}$  for  $\bar{T} = 0, 0.1$ . On the scale of this figure,  $m_\pi$  is insensitive to this variation of  $T$ . The current-quark mass is  $m = 0.011\eta$ , which for  $\eta = 1.06$  GeV yields  $M_\rho = 770$  MeV and  $m_\pi = 140$  MeV at  $T = 0 = \mu$ .

$$\int d^4x d^4y \bar{q}(x) \gamma_\mu \frac{\lambda^a}{2} q(x) g^2 D_{\mu\nu}(x-y) \bar{q}(y) \gamma_\nu \frac{\lambda^a}{2} q(y). \quad (25)$$

Field theories defined by such an interaction admit [ 18] a meson-diquark bosonisation that at tree-level predicts a mass for both mesons and diquarks. The procedure corresponds closely to solving the Bethe-Salpeter equations obtained by combining the ladder truncation of the quark-antiquark and quark-quark scattering kernels, depicted in Fig. 3, with the rainbow truncation of the quark DSE. Any form of  $g^2 D_{\mu\nu}(x-y)$  that is accurately able to reproduce the mass of the  $\pi$  and  $\rho$  mesons in this truncation will predict [ 19] the existence of stable, colour-antitriplet diquark bound states with masses:

$$m_{0^+}^{ud} \approx 740 \text{ MeV}, \quad m_{1^+}^{ud} \approx 950 \text{ MeV}, \quad m_{1^-}^{ud} \approx m_{0^-}^{ud} \approx 1500 \text{ MeV}. \quad (26)$$

This points to a possibly important attraction in the quark-quark channel.

However, it also presents a problem, of course, because asymptotic diquark states are not observed. The defect is in the truncation. [ 7] If one proceeds beyond the ladder-truncation in the quark-quark scattering kernel; e.g., including the other diagrams depicted in Fig. 3, one uncovers a repulsive contribution from the crossed-box diagram that eliminates the pole in the quark-quark scattering matrix; i.e., the full kernel does not support spurious diquark bound states. (The same procedure applied to  $SU(N_c = 2)$ -QCD predicts [ 20] that the mesons and diquarks are degenerate in that theory.) It is clear therefore that analyses of diquark correlations based solely on an effective interaction of the type in Eq. (25) can yield erroneous results, and the suggestion of diquark condensation may be amongst them.

The consequences of a putative diquark condensate are easy to elucidate. It is adequate to consider a simple separable model [ 21]

$$g^2 D_{\mu\nu}(\vec{p} - \vec{q}, \omega_k - \omega_l) := \delta_{\mu\nu} D_0 g(\vec{p}^2 + \omega_k^2) g(\vec{q}^2 + \omega_l^2), \quad g(k^2) := \exp(-k^2/\Lambda^2), \quad (27)$$

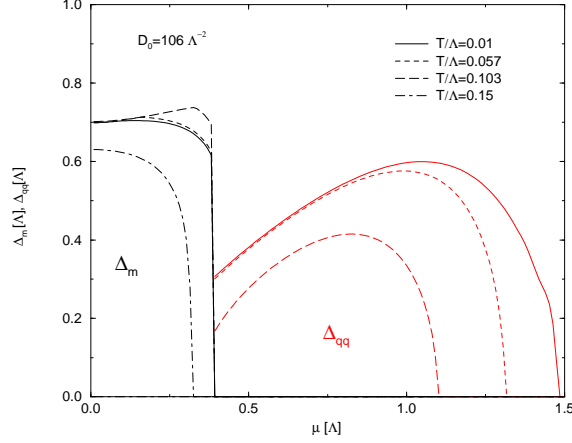


Figure 9. Quark and diquark mass gaps:  $\Delta_m, \Delta_{qq}$ .  $\Delta_{qq} \equiv 0$  at  $T = 0.15\Lambda$ ,  $\Lambda = 0.71$  GeV.

which preserves Goldstone's theorem and ensures the absence of a Lehmann representation for the quark propagator. This *Ansatz* has two parameters that can be fixed by requiring a good description of pion properties at  $T = 0 = \mu$ ; e.g.,  $D_0 = 106/\Lambda^2$ ,  $\Lambda = 0.71$  GeV yield  $f_\pi = 93$  MeV and  $-\langle \bar{q}q \rangle = (238 \text{ MeV})^3$ . A feature of the model is that it admits a semi-algebraic analysis and at  $\mu = 0$ , with these parameter values, it has second-order deconfinement and chiral symmetry restoration transitions at  $T_c \gtrsim 130$  MeV, while for  $T = 0$  these transitions are first-order at  $\mu_c = 330$  MeV neglecting the effect of a diquark condensate.

A meson-diquark bosonisation yields a tree-level auxiliary-field effective action whose extremum is determined by a pair of coupled equations for the quark and diquark mass gaps,  $\Delta_m$  and  $\Delta_{qq}$ :

$$\Delta_m = \Delta_m \frac{8}{3} D_0 T \sum_{l=-\infty}^{\infty} \int \frac{d^3 p}{(2\pi)^3} \frac{g^2(\tilde{p}_l^2)}{\epsilon_q(\tilde{p}_l^2)} \left[ \frac{\epsilon_q(\tilde{p}_l^2) + \mu}{\omega_l^2 + (\epsilon_q(\tilde{p}_l^2) + \mu)^2 + \epsilon_{qq}^2(\tilde{p}_l^2)} + \{\mu \rightarrow -\mu\} \right], \quad (28)$$

$$\Delta_{qq} = \Delta_{qq} \frac{4}{3} D_0 T \sum_{l=-\infty}^{\infty} \int \frac{d^3 p}{(2\pi)^3} g^2(\tilde{p}_l^2) \left[ \frac{1}{\omega_l^2 + (\epsilon_q(\tilde{p}_l^2) + \mu)^2 + \epsilon_{qq}^2(\tilde{p}_l^2)} + \{\mu \rightarrow -\mu\} \right], \quad (29)$$

with

$$\epsilon_q^2(\tilde{p}_l^2) = \vec{p}^2 + \Delta_m^2 g^2(\tilde{p}_l^2), \quad \epsilon_{qq}^2(\tilde{p}_l^2) = \Delta_{qq}^2 g^2(\tilde{p}_l^2). \quad (30)$$

The first equation arises from the confined-quark contribution to the effective action, while the second is the contribution from unconfined diquarks. The preliminary result of Ref. [21] for the  $(T, \mu)$ -dependence of  $\Delta_m$  and  $\Delta_{qq}$  is depicted in Fig. 9. The indications are that at  $T = 0$  there is a first order transition from a  $\Delta_m \neq 0$  phase to a  $\Delta_{qq} \neq 0$  phase at  $\mu \approx 280$  MeV. This behaviour persists until  $T \simeq 100$  MeV when only  $\Delta_m \neq 0$  is possible. There appears to be a tricritical point in the  $(T, \mu)$ -plane.

Clearly the formation of a diquark condensate is a simple and direct consequence of assuming that attraction dominates in the quark-quark scattering matrix. However, equally clearly, the validity of that assumption requires further consideration, with a first subject being the effect of the often-ignored repulsive terms in the quark-quark scattering kernel.

#### 4. CLOSING REMARKS

The DSEs are an efficacious tool for studying the strong interaction. In this application they expose the qualitative importance and quantitative effect of the nonperturbative dressing of propagators and vertices in QCD. The modelling involved is based on this observation, and it is necessary because of the need to make truncations. Questions will always be asked about the fidelity of that modelling, and the answers will come as more is learnt about about the constraints that Ward and Slavnov-Taylor identities in the theory can provide. That approach has already been particularly fruitful in QED,[ 22] and in the development of a systematic truncation procedure for the kernel of the quark DSE and meson BSE.[ 7, 20] In the meantime the judicious application of DSEs will continue to provide a flexible, intuition-building framework for the prediction, correlation and validation of observables.

#### REFERENCES

1. C. D. Roberts and A. G. Williams, *Prog. Part. Nucl. Phys.* **33** (1994) 477.
2. P. C. Tandy, *Prog. Part. Nucl. Phys.* **39** (1997) 477; C. D. Roberts, “Nonperturbative effects in QCD at Finite Temperature and Density”, nucl-th/9806088.
3. N. Brown and M.R. Pennington, *Phys. Rev. D* **39** (1989) 2723; M. R. Pennington, “Calculating hadronic properties in strong QCD”, hep-ph/9611242.
4. P. Maris and C. D. Roberts, *Phys. Rev. C* **56** (1997) 3369.
5. P. Maris and C. D. Roberts in *Rostock 1997, Progress in heavy quark physics*, edited by M. Beyer, T. Mannel and H. Schröder; nucl-th/9710062.
6. M. A. Ivanov, Yu. Kalinovsky, P. Maris and C. D. Roberts, *Phys. Rev. C* **57** (1998) 1991.
7. A. Bender, C. D. Roberts and L. v. Smekal, *Phys. Lett. B* **380** (1996) 7.
8. P. Maris and C. D. Roberts, “QCD bound states and their response to extremes of temperature and density”, nucl-th/9806005.
9. M. A. Pichowsky and T.-S. H. Lee, *Phys. Rev. D* **56** (1997) 1644.
10. M. Derrick, *et al.*, *Phys. Lett. B* **350** (1995) 120; S. Aid, *et al.*, *Nucl. Phys. B* **468** (1996) 3.
11. A. Bender, D. Blaschke, Yu. Kalinovsky and C.D. Roberts, *Phys. Rev. Lett.* **77** (1996) 3724.
12. P. Maris, *Phys. Rev. D* **52** (1995) 6087.
13. D. Blaschke, A. Höll, C. D. Roberts and S. Schmidt, “Analysis of chiral and thermal susceptibilities”, *Phys. Rev. C*, in press, nucl-th/9803030.
14. A. Höll, P. Maris and C. D. Roberts, in progress.
15. D. Blaschke, C.D. Roberts and S. Schmidt, *Phys. Lett. B* **425** (1998) 232.
16. A. Bender, *et al.*, *Phys. Lett. B* **431** (1998) 263.
17. P. Maris, C. D. Roberts and S. Schmidt, *Phys. Rev. C* **57** (1998) R2821.
18. R. T. Cahill, J. Praschifka and C. J. Burden, *Aust. J. Phys.* **42** (1989) 161; R. T. Cahill, *ibid* 171.
19. C. J. Burden, *et al.*, *Phys. Rev. C* **55** (1997) 2649.
20. C. D. Roberts in *Quark Confinement and the Hadron Spectrum II*, edited by N. Brambilla and G. M. Prosperi (World Scientific, Singapore, 1997).

21. D. Blaschke, Yu. L. Kalinovsky and B. Van den Bossche, “Diquark condensation and deconfinement in the quark matter phase diagram”, in progress.
22. A. Bashir, A. Kizilersu and M.R. Pennington, *Phys. Rev. D* **57** (1998) 1242.